ADVANCED BIOSYSTEMS
www.adv-biosys.com

Manipulation of Single Cells Using a Ferromagnetic Nanorod Cluster Actuated by Weak AC Magnetic Fields

*Lu Zhu, Weijie Huang, Fengchang Yang, Lei Yin, Shenxuan Liang, Wujun Zhao, Leidong Mao, Xiaozhong (John) Yu, Rui Qiao, and Yiping Zhao**

A unique noncontact single cell manipulation technique based on the actuation of magnetic nanorods (MNRs) or clusters (MCs) by nonuniform alternating magnetic fields (nuAMFs) is demonstrated. Compared to the actuation of MNRs/MCs by conventional magnetophoresis, the motion of MNRs/MCs actuated by nuAMFs can be tuned by additional parameters including the shape of MNRs/MCs and the frequency of the applied magnetic fields. The manipulation of a single cell by an actuated MNR/MC are divided into five stages, i.e., approaching, pushing, carrying, dragging, and releasing. The interactions between the MNR/MC and the cell in these stages are investigated in detail both experimentally and numerically. Other applications of cell manipulation, such as concentrating cells at target locations and accumulating MNRs/MCs onto a single cell, are also demonstrated. The single cell manipulation system is simple, low-cost, and low-power consumption, and helps advance the state-of-the-art of single-particle manipulation.

1. Introduction

Single-cell manipulation has great potential for biology study but is a great challenge for bioengineering. In the past decades, many single-cell manipulation techniques have been developed, e.g., optical tweezers,[1,2] atomic force microscopy,[3] electrophoresis,[4] and magnetic robotics.[5,6] These methods have shown great potential in cell targeting, migrating, and positioning, and enable the interactions between cells and their environment to be explored in details. They also have potentials in medical applications such as targeted drug delivery and disease diagnostics. For these applications, the high-precision manipulation of micro/nanoparticles in liquid environments is an essential operation. However, the application of the existing tools for single-cell manipulation is often limited by their high cost, device complexity, and biocompatibility.

Among the aforementioned methods, those based on magnetic field (B-field) offer inherent advantages such as multifunctionality, targetability, and controllability. A majority of these manipulation methods are based on magnetophoresis, in which magnetic particles move toward position with stronger field strength in nonuniform B-fields. Nonmagnetic particles/cells can be manipulated magnetically by tethering magnetic particles to cells or by using a specially designed magnetic structure to drive them.[5–10] For example, by labeling HeLa cells with magnetic nanoparticles, Ho et al. prepared magnetic multicellular spheroids and demonstrated cell separation by applying a B-field, without the need of centrifugation.[11] Similarly, Ino et al. patterned magnetically labeled single cells into lines by using magnetite nanoparticles and magnetic forces.[12] Magnetically functionalized cells were also assembled under external magnetic fields and grew into tissues.[13–15] Magnetic microstructures have also been investigated as transporters for single cells. For example, Sakar et al. fabricated U-shaped Fe_3O_4 microtransporters to manipulate Tetrahymena pyriformis cells.[6] The dead cells were separated individually without disturbing the local environment. Sophisticated, on-chip integrated microelectromagnet (MEM) systems can be used to manipulate, separate, and trap cells into 2D arrays for high throughput analysis.[16–23] For instance, Lee et al. developed a microeletromagnet matrix to manipulate and sort

Dr. L. Zhu
School of Chemical
Materials and Biomedical Engineering
College of Engineering
University of Georgia
Athens, GA 30602, USA
Dr. W. Huang, Prof. Y. Zhao
Department of Physics and Astronomy
University of Georgia
Athens, GA 30602, USA
E-mail: zhaoy@uga.edu
Dr. F. Yang, Prof. R. Qiao
Department of Mechanical Engineering
Virginia Tech
Blacksburg, VA 24061, USA
Dr. F. Yang
JENSEN HUGHES, Inc.
Blacksburg, VA 24060, USA
Dr. L. Yin, S. Liang, Prof. X. Yu
College of Public Health
University of Georgia
Athens, GA 30602, USA
Dr. W. Zhao, Prof. L. Mao
School of Electrical and Computer Engineering
College of Engineering
University of Georgia
Athens, GA 30602, USA
The ORCID identification number(s) for the author(s) of this article can be found under https://doi.org/10.1002/adbi.201800246.

DOI: 10.1002/adbi.201800246

individual cells.[19] The matrix consists of two perpendicularly positioned layers of Au wires, and by changing the current in each wire, a versatile B-field could be generated to manipulate cells attached on magnetic beads. Despite its success, MEM as a cell manipulation technique also faces two major issues. First, to generate field gradients strong enough for cell manipulation, a large current through the wire grid must be used. Such a large current generates significant Joule heat, which often requires additional cooling system to be attached to the integrated chip. Second, the high current density also implies that the cross-section of the microwires should be large enough to avoid any electromigration, which limits the density of the array and the compactness of MEM. Because of these issues, the fabrication and substrate structure of MEM are often complicated, and the operation of MEM requires high-current power supplies, both of which tend to increase the cost and compromise the device reliability. In addition, the technical attributes of an ideal single cell manipulation method include high resolution in 2D/3D space, dexterity (i.e., ability to move a particle along an arbitrary path), high throughput, and robustness. Different applications often demand different attributes, e.g., some single-cell analysis requires dexterity and high spatial resolution in 2D space, while other analysis requires modest spatial resolution but high throughput.[24] Importantly, the success of a manipulation method is often limited by its nontechnical attributes. For example, in single-cell analysis, biocompatibility is critical and the ease of integrating a cell manipulation device into a cell study platform is often a crucial consideration. Finally, cost is often a decisive factor, especially for resource-limited research and education communities.

In our recent work,[25] actuation of magnetic nanorods (MNRs) or magnetic clusters (MCs) by a nonuniform alternating magnetic field (nuAMF) has been achieved. Different from a permanent magnet pulling a magnetic particle, it is demonstrated that the MNRs or MCs move away from the magnetic source under the nuAMF, and there is a periodic fluctuation of speed during the movement of MC. The fluctuation has a frequency twice the frequency of the applied B-field. The speed of an MC actuated by a nuAMF can be changed by varying the frequency or current supplied to the solenoid.[25] Comparing to conventional magnetophoresis that uses B-field gradient to move an MC, the motion of an MC under the nuAMF can be manipulated by more parameters, which offers more flexibility in practical applications. We have found that moving an MC using the nuAMF with the same speed requires much smaller current in the electromagnetic system as compared to that required by DC field-gradient-based magnetophoresis. As shown in Figure S1 of the Supporting Information, to achieve the same speed (≈0.92 μm s^{-1}) for an MC with an effective size of 20 μm, using the same solenoid, a DC B-field needs a 5 A current while the nuAMF only needs a current amplitude of 0.44 A, i.e., the power consumed by the nuAMF is about 0.39% of that by the DC B-field. Thus, in addition to the positive attributes afforded by conventional magnetophoresis-based methods, using an MC actuated by a nuAMF to manipulate the motion of nonmagnetic particles could provide additional advantages such as simplicity of device, simplicity of control, and greatly reduced power consumption.

Here we will show that with a programmable keyboard to control four solenoids, an MNR/MC can be actuated by a nuAMF to execute highly directional motion with submicrometer lateral resolution. The magnetically actuated MC can be further used to manipulate single cells in liquid environment. The manipulation process can be divided into five stages, i.e., approaching, pushing, carrying, dragging, and releasing. During the manipulation, the MC and cell are not in physical contact and the cell manipulation originates from the hydrodynamic interactions between the cell and the actuated MC. The effect of the frequency of the applied B-field on the manipulation behavior is investigated in detail. Operations such as concentrating cells at a desired location, accumulation MCs onto a single cell are also demonstrated.

2. Results and Discussion

2.1. The Controlled Motion of a Single MNR

Before using the MNR/MC to manipulate single cells, the performance of magnetic manipulation system and the motion of a single MNR/MC were investigated systematically. As shown in our previous report,[25] the translational moving speed of an MNR/MC is governed by the size and shape of the MNR/MC as well as the strength (i.e., the current amplitude of the solenoid I_0) and the frequency f_H of the B-field. In addition, for manipulation purpose, the motion of the MNR/MC should also be characterized by two other parameters: the directionality and precision of its translational motion. These two parameters are influenced by the thermal fluctuation (i.e., Brownian motion) of the MNR/MC in liquid, noise in nuAMF signals and/or hydrodynamic boundary conditions. In fact, in the practice of single cell manipulation, the size and shape of the MNR/MC will be fixed while the field conditions is optimized. Thus, without losing the generality, here we focused on the Ni MNRs since they have a fixed shape and size. We also fixed the current amplitude $I_0 = 2$ A for the solenoid, and varied the field frequency f_H as well as the current on–off duty cycles. As we will see later, the MCs we used to manipulate cells (**Figure 1**b) is much larger than the Ni MNRs (Figure 1a), so it is expected that the effect of Brownian motion on the motion of an MC would be much reduced compared to that of a Ni MNR.

The directionality of an MNR's motion is defined in **Figure 2** with respect to a reference vector given by the B-field direction $\hat{\boldsymbol{B}}$ (the red vector in Figure 2). The trajectory of an MNR over a period Δt is divided into N equal time sections. Within the ith section, a section displacement vector r_i is defined to point from the MNR's initial location toward its final location (green vectors in Figure 2). The angle θ_i between r_i and $\hat{\boldsymbol{B}}$, $\cos\theta_i = \boldsymbol{r}_i \cdot \hat{\boldsymbol{B}}/|\boldsymbol{r}_i|$, gives the local directionality of the motion. Two parameters can be used to characterize the directionality of the MNR's motion over a time period Δt: an average directionality defined as $D_\mathrm{d} = \frac{1}{N}\sum_{i=1}^{N}\cos\theta_i$, or the standard

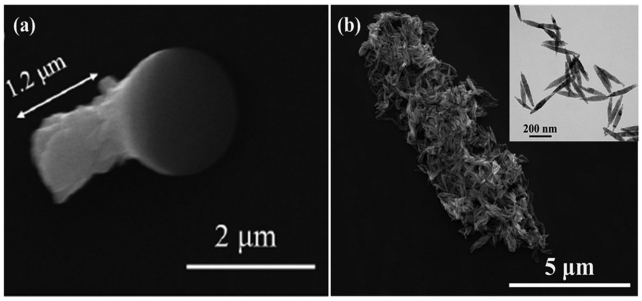

Figure 1. a) A representative scanning electron microscope (SEM) image of a single Ni nanorod. The sphere is a PS bead. b) A representative SEM image of a Fe_3O_4 nanorod cluster. The inset is a TEM image of Fe_3O_4 nanorods.

deviation $\Delta\theta$ of the distribution of θ_i. When the MNR's translational motion exactly follows the direction of the B-field, $D_d = 1$, indicating a prefect directionality. When the MNR performs a random motion, $D_d = 0$. **Figure 3**a shows the measured D_d and $\Delta\theta$ at four different B-field frequencies (f_H = 5, 10, 20, 40 Hz) obtained from 10 s trajectories of a single Ni MNR actuated by a nuAMF. For each data point, at least five trajectories were analyzed and averaged. The corresponding histogram of θ_i and the normal distribution fitting are shown in Figure S3a of the Supporting Information. The result indicates that, when f_H increases from 5 to 20 Hz, $\Delta\theta$ decreases while D_d increases; when f_H > 20 Hz, $\Delta\theta$ increases and D_d decreases. Therefore, B-fields with a frequency of f_H = 20 Hz (also statistically f_H = 10 Hz) gives the best directionality of $D_d = 0.8 \pm 0.1$.

The directionality D_d is closely related to the speed υ of the MNR. The displacement $\vec{s}$ of an MNR can be divided into two parts

$$\vec{s} = \vec{s}_T + \vec{s}_B, \tag{1}$$

where $\vec{s}_T = \upsilon t$ is the directional displacement driven by the nuAMF and shall be parallel to direction of $\vec{B}$, while $\vec{s}_B$ is the random displacement caused by the Brownian motion (or other noises in the system) and its mean-squared displacement

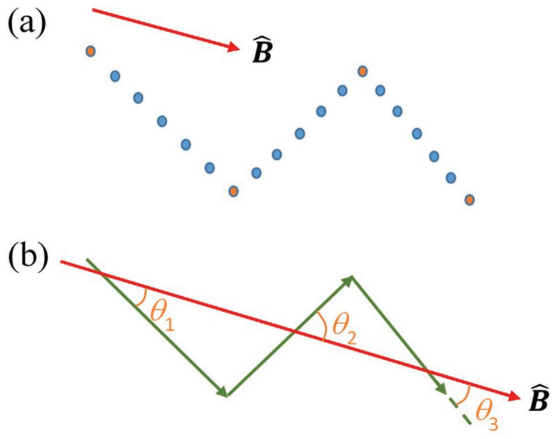

Figure 2. a) Illustration of a trajectory of an MNR move under a nonuniform AC B-field. b) The definition of the directionality angles.

is $\langle|\vec{s}_B|\rangle = \sqrt{4Dt}$, where D is the diffusion constant of the MNR in liquid.[26] If $|\vec{s}_T| \gg |\vec{s}_B|$, i.e., $\upsilon = |\frac{d\vec{s}}{dt}|$ is large, the movement of an MNR is dominated by its directional motion, and one could ignore the Brownian motion and thus D_d approaches to 1. In the opposite limit of $|\vec{s}_T| \ll |\vec{s}_B|$, D_d approaches to 0. The relationship between D_d and υ can be simulated by assuming the MNR as a sphere, and the result is shown in Figure S3b of the Supporting Information (the directional motion parameters are taken from the experimental data of f_H = 20 Hz). Figure 3b shows the experimentally measured D_d and υ versus f_H for a Ni MNR, both $D_d - f_H$ and $\upsilon - f_H$ relationship show similar trend with a small discrepancy, implying a positive correlation. The optimal D_d is obtained at f_H = 20 Hz, but the fastest moving speed υ occurs at f_H = 40 Hz.

To control the motion of an MNR in a 2D plane, the B-field generated by the four solenoids needs to be turned on and off from time to time (see below). It is expected that the on–off time (duty cycle) could affect the motion of the MNR. Thus, a systematic investigation has been carried out. As shown in Figure 3c, a window function was applied to a continuous sinusoidal signal for a fixed f_H = 20 Hz (period T = 0.05 s), with an "on" time period t_s and an "off" time period t_0. Two sets of experiments have been carried out: to set $t_s = t_0$ but vary t_s and to fix t_0 = 0.5 s but change t_s from 0.01 s to 0.5 s. Figure 3d shows the effective speed υ of an MNR versus t_s for the two cases, $t_s = t_0$ and a fixed t_0 = 0.5 s. When $t_s = t_0$, it is observed that when $t_s \leq T$, where $T = 1/f_H$, the speed υ increases with t_s; while when $t_s > T$, the speed υ is almost a constant. In particular, when $t_s \sim T/2$, the speed υ reaches a maximum. This shows that a particular phase modulation of the sinusoidal signal would significantly change the translational speed. When t_0 is fixed at 0.5 s (>>T), the speed υ is significantly affected by the ratio of t_s:t_0. When $t_s < t_0$, i.e., when t_s < 0.1 s, the speed υ fluctuates greatly with t_s. This is because when $t_s < t_0$, $|\vec{s}_T| \ll |\vec{s}_B|$ or $|\vec{s}_T| \sim |\vec{s}_B|$, and the Brownian motion will play a significant role in the translational motion. However, when t_s is large enough,, i.e., when the ratio of t_s:t_0 approaches to 1 or when t_s > 0.1, $|\vec{s}_T| > |\vec{s}_B|$, the motion is dominated by the directional motion, and the speed υ reaches a constant, which approaches to the speed of the MNR under a continuous sinusoidal signal.

Clearly, one of the best conditions to control the translational motion of a single Ni MNR using a nuAMF in our setup is to set f_H = 20 Hz or 10 Hz while keeping I_0 = 2 A for the solenoid, and making sure that t_s is large enough. Since an MNR can be actuated by a nuAMF, and it moves away from the solenoid, if one could set up two pairs of solenoids in orthogonal horizontal x–y plane, and by programming the four solenoids with on–off AC currents, one could control the motion of a Ni MNR to follow a desired trajectory. **Figure 4** shows three letters, "U," "G," and "A," traced by the trajectories of a Ni MNR actuated using our four-soneloid system (see Section S2 in the Supporting Information for the setup) and the corresponding trajectory movies are shown in Movie S2 of the Supporting Information. The inset in the upright corner shows the predesigned pattern which is a 32 × 32 pixel black-white image. Compared to the designed letters, the squareness of the trajectory needs to be further

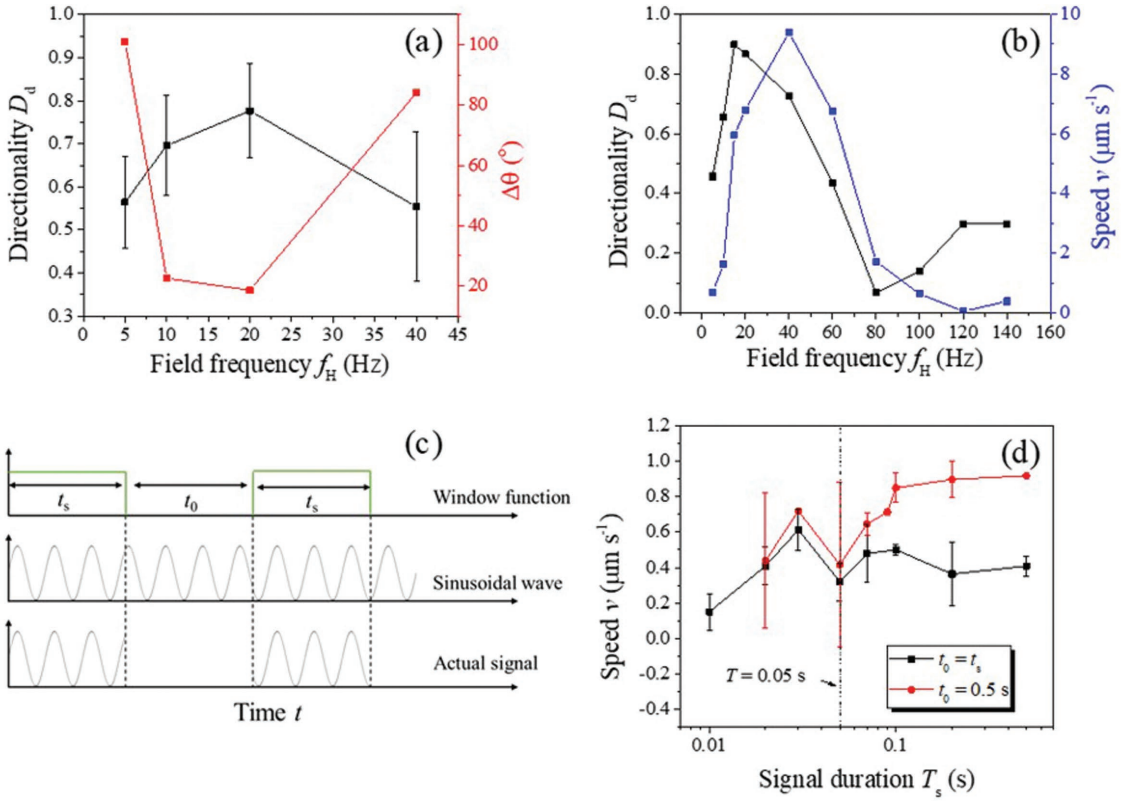

Figure 3. a) The plots of directionality D_d and width of deviated angle distribution $\Delta\theta$ versus f_H of a Ni MNR for a continuous nonuniform AC B-field (nuAMF). b) The plots of directionality D_d and speed v versus f_H of a Ni MNR for a continuous nuAMF. Motion study with noncontinuous nuAMF signal. c) Illustration of the noncontinuous sinusoidal signal by applying a window function to a continuous sinusoidal signal. d) The plot of the average speed v versus the "on" time duration t_s for two cases: $t_s = t_0$ and a fixed $t_0 = 0.5$ s.

optimized. Nevertheless, these trajectories clearly demonstrate the controllability of the motion of an MNR actuated by a nuAMF.

2.2. The Manipulation of a Single Cell

Since an MNR/MC can be actuated using a nuAMF in a precision and controllable fashion, we use it to control the motion of another particle. Movie S3 of the Supporting Information shows a typical example using an MC to move a single PC3 cell. The MC formed by Fe_3O_4 MNRs was ≈20 μm in length and ≈13 μm in width. During the manipulation process, a nuAMF with a current amplitude $I_0 = 2$ A and $f_H = 10$ Hz was applied. Clearly, the cell could move along with the MC and its moving direction was controlled by the MC's moving direction. By investigating the entire moving process, we found that the interactions between an MC and the targeted cell can be divided into five stages as shown in **Figure 5**: the MC approaching to the cell (Stage I), pushing the cell (Stage II), carrying the cell (Stage III), dragging the cell (Stage IV), and releasing the cell (Stage V), respectively. In the beginning, when the distance between the

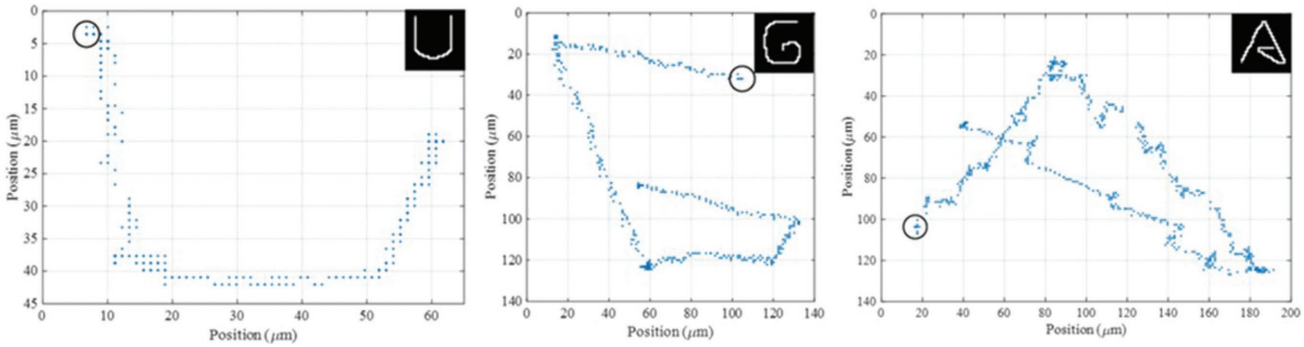

Figure 4. Letters "U," "G," and "A" traced by a Ni MNR actuated by a nonuniform AC B-field ($I_0 = 2$ A, $f_H = 20$ Hz, $t_s = 0.2$ s, and $t_0 = 0.5$ s).

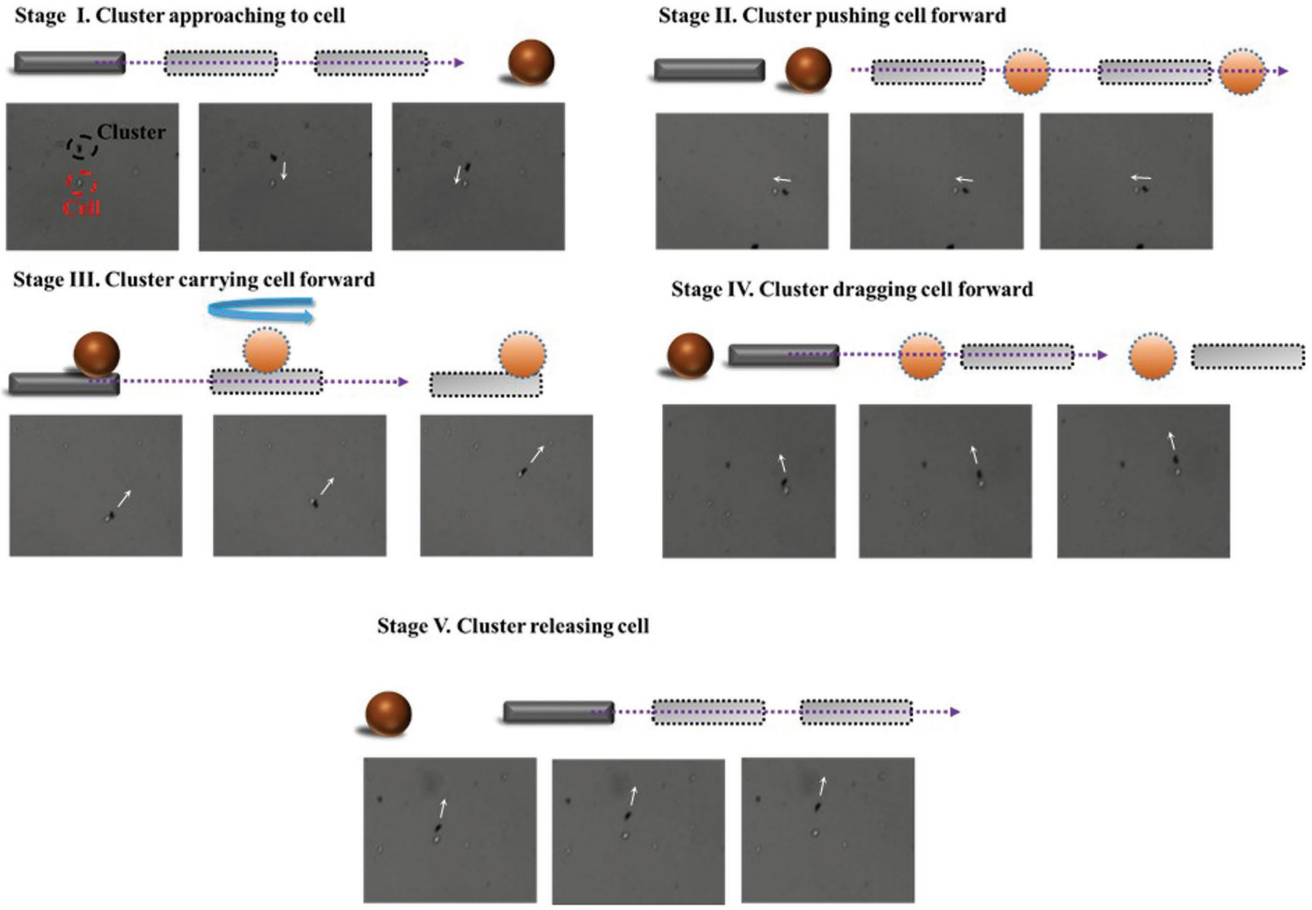

Figure 5. Illustration of the five stages of cell manipulation and corresponding snapshots. Stage I: Approaching; Stage II: Pushing; Stage III: Carrying; Stage IV: Carrying; and Stage V: Releasing. The arrows in the photos indicate the MC's moving direction.

MC and the target cell was large, the MC was moving toward the cell without disturbing the cell (Figure 5, Stage I). When the distance in between the cell and the MC became small enough, the MC started to approach the cell quickly and push the cell forward (Figure 5, Stage II). In the meantime, the distance between the cell and the MC decreases. When the MC appeared to get "in touch" with the cell (experimentally the separation between the MC and the cell could not be resolved under the optical microscope, but in fact the MC and the cell are not physically in contact as we will explain later), it started to carry the cell moving away from the control solenoid (Figure 5, Stage III). During the carrying process, the cell was oscillating along the surface of the cluster, which was caused by the rotation of the MC under the alternating B-field. However, the carrying process can break down sometimes if the distance between the cell and the MC were large enough the carrying process stopped and the MC started to drag the cell forward (Figure 5, Stage VI). During the dragging process, the distance between the MC and the cell continuously increases. If the magnetic field is quickly switched from y- (x-) direction to x- (y-) direction so that the MC would gain a speed to move away from the cell, depending on the relative locations of MC and cell and the cell moving direction, eventually the MC released the cell and moved away (Figure 5, Stage V), and the cell stayed at where it was released.

Figure 6 shows the trajectories of the MC and the cell, their displacements/accumulative travel distances (s' for the MC and s for the cell), and their separation (Δs) as a function of time obtained from Movie S3 of the Supporting Information. The corresponding interaction stages are also labeled in Figure 6. Note that the cell has a diameter of ≈10.5 µm. As shown in the trajectory plot of Figure 6a, initially, the MC and the cell were far away from each other, the trajectory of MC was directed toward the cell location, while the trajectory of cell showed a random motion. Once the MC was approaching toward the cell within a critical distance (the cell center to the MC center distance of ≈30 µm), the MC started to push the cell forward (Stage II). During the pushing stage, the cell slid to the right side of the MC, and moved along with the MC in an almost parallel fashion (Stage III). A wavy trajectory appeared for the cell indicated that the cell was oscillating along the surface of MC, which is also clearly showed in the relative distance Δs plot and the displacement plot of the cell in Figure 6b. As for the MC, it moved almost straight forward. At a certain time, the MC started to lead the cell. The cell followed the MC for a short time and it shifted to the left side of the MC during this time. As the MC moved forward further, the separation between the MC and the cell became larger and larger, and eventually the cell stopped to move while the MC still moved forward, i.e., the cell was released.

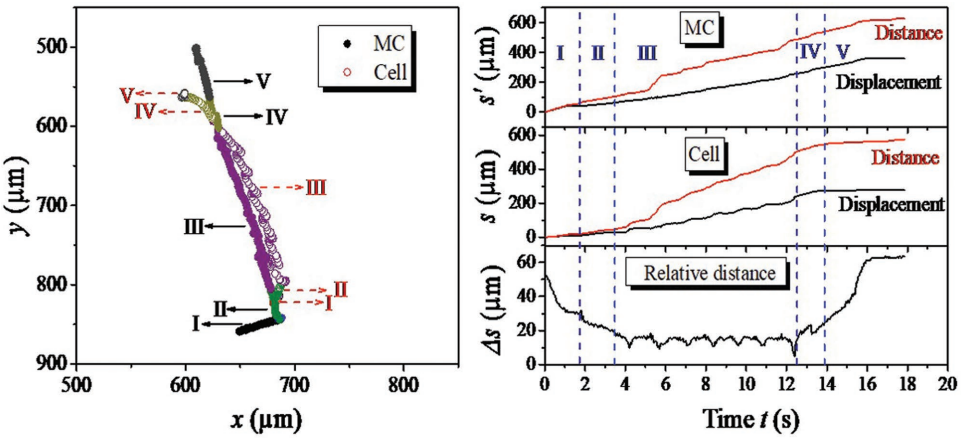

Figure 6. a) Representative trajectories of an MC and a PC3 cell at f_H = 10 Hz (different colored symbols represent different stages), and b) MC/cell moving distance/displacement and separation between the cell and the MC. The Roman numerals "I"–"V" represent each cell manipulation stage labeled in Figure 5.

Similar behaviors can be seen from the displacement/distance plots for the MC and the cell shown in Figure 6b. The separation Δs versus manipulation time t plot can give more quantitative information. The initial separation Δs ($t = 0$) between the cell and the MC was 52.3 μm. At $t \approx 0.8$ s, Δs decreased to ≈30.9 μm, and stayed in this value for ≈1 s till the MC started to push the cell forward. In Stage II ($t \geq 1.8$ s), Δs decreased continuously from ≈31 to ≈19 μm at $t = 2.5$ s. Then the cell moved to the right side of the MC, and was carried to move forward in Stage III. The Δs oscillated periodically between ≈18 and ≈9 μm with a period of ≈1.3 s. At $t = 12.5$ s, Δs reached a minimum of ≈9 μm where the MC and the cell appeared almost overlapped with each other. At $t > 12.5$ s, the MC quickly led the cell, and Δs rapidly reaches to 19.7 μm, and the cell moved along with the MC for ≈1.5 s. At $t \approx 14$ s, Δs increased almost linearly with t, which indicated that the MC and the cell were disengaged.

Since the translational motion of a rotating MC in nuAMF is induced by its hydrodynamic interactions with the stationary wall,[25] hydrodynamic interactions may also play a key role in the noncontact manipulation of cells by an actuated MC. Hence, to understand cell manipulation by an actuated MC, we examine the 3D fluid flow near an MC using numerical simulations. The simulation system consists of an MC and a cell immersed in a liquid film positioned on a solid substrate as shown in **Figure 7**. The geometrical centers of the MC and cell are positioned at z_{MC} and z_{cell} above the substrate, respectively. The cell is placed at various lateral and longitudinal offsets (Δx and Δy) with respect to the MC's geometrical center. The MC is modeled as a cylinder with each end covered by a hemisphere. Similar to those in our experiments, the long and short axes of the MC are 20 and 13 μm, respectively. The cell is modeled as a rigid sphere with a diameter of 10.5 μm. The dimension of the simulation domain measures 300, 200, and 100 μm in x-, y-, and z-directions. Our prior work showed that, driven by a nuAMF, the movement of an MC near a solid substrate is induced by its out-of-plane rotation.[25] Since the MC's translation speed varies only weakly during cell manipulation (Figure 6), as a first approximation, the MC is assumed to move at a constant velocity of v_T and rotate at a constant rate of $\bar{\omega}$. The fluid flow near the moving MC and the hydrodynamic force experienced by the cell is solved using a commercial finite-element package COMSOL (see Section S5 in the Supporting Information for details).[27]

Figure 7b shows the hydrodynamic force (F_x) experienced by a cell along the direction of the MC's translation when the cell is positioned at different longitudinal offset Δx with respect to the MC (its lateral offset is fixed to $\Delta y = 0$). The height of the MC and cell, z_{MC} and z_{cell}, are 10.5 and 5.5 μm above the substrate, and the results are qualitatively similar for other choices of z_{MC} and z_{cell}. We observe that, regardless of whether the cell is in front of or behind the MC, it experiences a force that drives it to move along with the MC. This force originates from the imbalance of the pressure on the front and rear surface of the cell, which is in turn induced by the movement of the MC (see Figure S6, Supporting Information). This positive force explains why a moving MC can "push" a cell forward during Stage II when it is moving behind the cell. Similarly, this force also explains why a moving MC can "pull" a cell forward during Stage IV. This force decreases rapidly as the longitudinal offset between the cell and the MC increases, e.g., as Δx increases from 20 to 50 μm, F_x decreases by a factor of 6.6, indicating that the ability of an MC to push/pull a cell decreases rapidly as their separation increases. This helps explain why noticeable movement of cell occurs only when an MC approaches closely (≈20 μm in our experiments).

The transition of cell manipulation from Stage II to Stage III occurs when a cell moves to the side of the MC and travels with it. This transition can be attributed to the fact that, in the experiments, the cell and the MC are not always exactly aligned (i.e., the cell may have nonzero lateral offset Δy). At a finite lateral offset, the flow induced by a moving MC generates a hydrodynamic force on the cell to drive it to move laterally with respect to the MC. To see this clearly, a cell is fixed at longitudinal and lateral offsets of 30 and 5 μm with respect to the moving MC. Other conditions, e.g., the vertical positions of the cell and the MC, and the speed of the MC, are identical to those used in Figure 7. **Figure 8** shows the velocity and pressure fields of

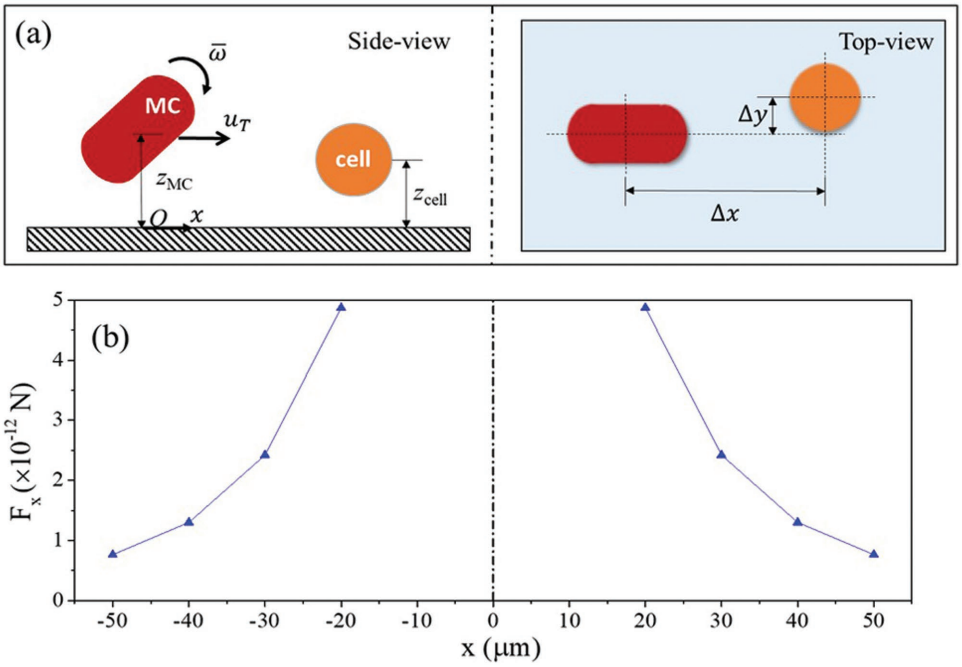

Figure 7. a) The side and top views of the system used to study the hydrodynamic interactions between a moving MC and a cell fixed at various longitudinal and lateral offsets (Δx and Δy) with respect to the MC. b) The x-direction hydrodynamic force experienced by a cell as a function of its longitudinal offset with respect to the MC ($\Delta y = 0$, $z_{MC} = 10.5$ μm, $z_{cell} = 5.5$ μm, $u_T = 35$ μm s^{-1}, $\bar{\omega} = 31.4$ s^{-1}).

the fluids near the cell in an x–y plane passing through the cell's center. Because the flow induced by the MC is diverted around the cell, positioned slightly off its moving direction, the pressure on the cell surface facing the MC is slightly higher than that on the surface away from the MC. Such a pressure difference creates a force on the cell that pushes the cell aside (see Figure 8), as observed experimentally during the transition of cell manipulation from Stage II (pushing) to III (carrying). Clearly, our theoretical models demonstrate that the hydrodynamic interactions between the MC and the cell allow a cell to be manipulated effectively by an actuated MC without requiring the MC to contact the cell physically. Experimentally, considering the size of the MC and the cell as well as the projected 3D configuration of MC and cell into a 2D movie, there could be always a gap between the MC and the cell, i.e., the two particles may not in any kind of physical contact during our observations.

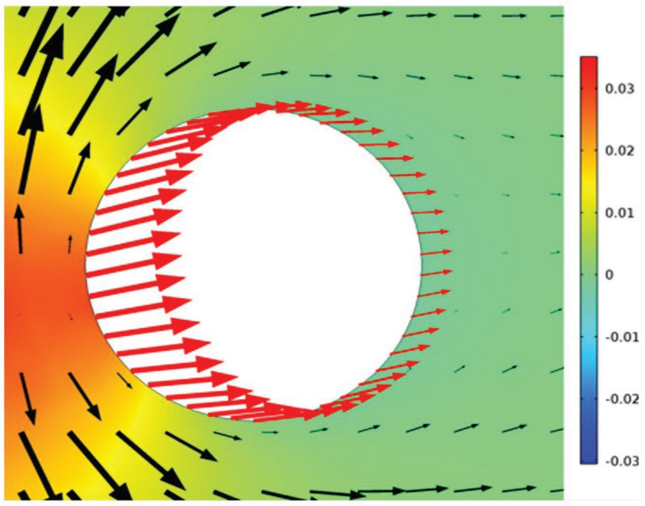

Figure 8. The velocity field (black arrows) and pressure field (color-coded) near a cell manipulated by an MC. The hydrodynamic force on the cell surface is labeled using red arrows. All hydrodynamic observables are shown in the xy-plane passing through the cell's center. The cell is positioned with longitudinal and lateral offsets of 30 and 5 μm with respect to the MC, respectively. Other simulation conditions are identical to those used in Figure 7.

Such an observation demonstrates that the current method has a great advantage for cell manipulation over other magnetophoresis techniques. As we briefly reviewed in Section 1, so far most cell manipulation techniques based on the magnetophoresis principle have to first make the cell magnetic either by coating the cells with magnetic particles or ingesting magnetic nanoparticle into the cells.[5–10] The addition of particles on cell surfaces or inside cells inherently changes the cell performance, and care needs to be paid to interpret the activity of the cells after manipulation or extra works has to be done in order to remove the magnetic particles from cells. The magnetic transporter method using static magnetic field gradient does not require the modification of cells, but the transporter has to be in direct contact with the cells, which could cause additional mechanical damage to cell membrane.[6] For the manipulation method reported here, since the interaction between the MC and the cell is hydrodynamic due to the flow field induced by the rotation of the MC, so that when the cell is manipulated by the MC, the cell and the MC are not physically in contact. Therefore, the cell shall have its full original functionality during/after the manipulation, which can perform normal cell activity after manipulation.

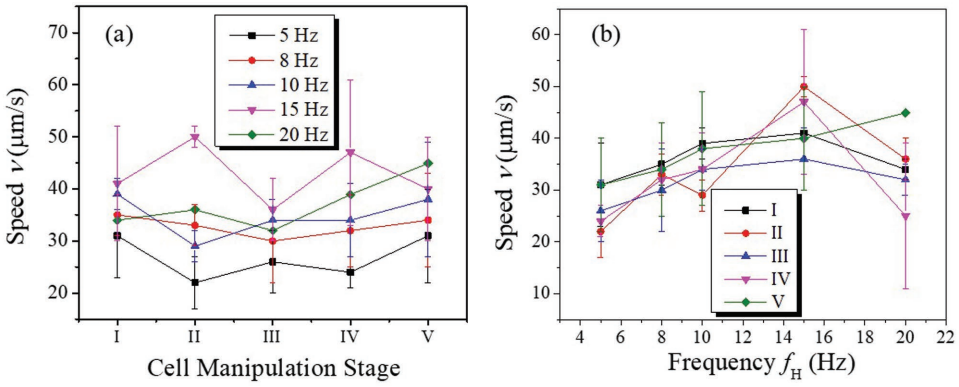

Figure 9. a) Comparison of the speed of the MC at different cell manipulation stages for different f_H; and b) the plot of the speed of the MC versus f_H at different cell manipulation stages.

In addition, a systematic investigation on how f_H affects the cell manipulation has been performed for a fixed I_0 = 2 A. By analyzing the trajectories of both the MC and the cell, we find that they also follow the five stages described in Figures 5 and 6. Without losing the generality, we tracked the speed v_{MC} of the MC at different manipulation stage under different f_H to characterize the manipulation performance, as shown in **Figure 9**. Two distinguished trends can be found: First, for the same f_H, regardless of the cell manipulation stage, v_{MC} is statistically a constant, though in some cases a weak trend of higher v_{MC} at Stages I and V is visible (Figure 9a). Second, when f_H increases from 5 to 15 Hz, v_{MC} in all stages increases monotonically with f_H; when f_H reaches up to 20 Hz, v_{MC} in all stages decreases abruptly (Figure 9b). Such a behavior is consistent with the motion behavior of a single MC as reported previously, where a critical f_H exists for the motion of an MC; when f_H is less than the critical value, v_{MC} increases monotonically with f_H; when f_H is larger than the critical value, v_{MC} decreases with f_H.[25] However, for the size of the MC used in our cell manipulation experiment (with a projection area ≈260 μm^2), the reported critical f_H value for a single MC is ≈60 Hz while in the current cell manipulation experiments, this value is between 15 and 20 Hz. Such a reduction of the critical f_H value could be a result of the hydrodynamic interactions between the MC and the cell as we discussed above.

2.3. Other Cell Manipulation Applications

Using an MC actuated by nuAMFs to manipulate a single cell is a versatile technique with simple and inexpensive setup as discussed above. Based on this technique, other cell-related application can be demonstrated. For example, using an MC to collect multiple cells to a small area is feasible. In this experiment, a mixture of MC suspension with a PC3 cell suspension was used with I_0 = 2 A and f_H = 8 Hz. A single elongated MC (≈52 μm in length and 15 μm in width) was repeatedly actuated by our control system to move cells spread on the surface to the upper left corner, and as an evidence in the corresponding movie (Movie S3, Supporting Information) and the representative movie frames in **Figure 10**. As shown in Figure 10a, initially cells (the light-colored particles in the figure) were distributed randomly on a Si substrate, and in the marked black circle there were only five cells (including a three-cell cluster). By actuating the MC, the cell in yellow-dotted circle of Figure 10a was brought into the close-by location of the three-cell cluster, and was released; then the MC was moved to the cell in red-dotted circle of Figure 10a, and again moved that cell to a location near the three-cell cluster. Figure 10b shows the trajectories of the two cells and their final locations. By repeating this process, more and more cells could be moved to the black-circled area as shown in Figures 10c–e: at t = 3 min, 10 cells were collected; at t = 5 min, 13 cells were collected; and finally at t = 9 min, most cells (16 cells) in the field of view were moved to the target area.

Cell manipulation can only be achieved when the cells are not fixed onto the substrates. However, if the cells are fixed onto the substrates, an alternative application, accumulating MCs onto a single cell, can be performed. In the work of Wang et al., novel "nanopearl-necklace" structured multifunctional nanoparticles were fabricated and their imaging/photothermal ablation abilities of cancer cells were investigated.[28] After linking the antibodies onto the surface of Au_{rod}–Fe_3O_4 nanopearl-necklace probes, they can be used to target the human breast cancer SK-BR-3 cells. With the irradiation of 718 nm NIR laser, the deaths of targeted cells were observed. The work of Kim et al. proposed a new method to rupture the cancer cells.[9] Magnetic microdisks were biofunctionalized with antihuman-IL13α2R antibodies to target human glioblastoma cells. After targeting the cancer cells, when an alternating (AC) magnetic field was applied, the magnetic disks started to oscillate, which compromised cell membrane's integrity and initiated spin-vortex-mediated, programmed cell death.[9] Thus, it is also important to understand the how the amount of magnetic nanoparticles or MNRs on the cell affect the treatment.

Using the nuAMF actuation method, we demonstrated that one can accumulate one MC a time onto a single cell, which can lay foundation for future single cell imaging/drug delivery study. Here, the lung cancer cell, A549 cell, was used to demonstrate the idea. When an A549 cell suspension was dispensed onto a Si substrate, the cells start to grow and adhere to the substrate. As shown in Movie S4 of the Supporting Information or snapshots in **Figure 11**, when an MC was moved close to a fixed cell, it would be attached to the cell surface, presumably due to electrostatic or van der Walls interactions (Figure 11a). Once the MC stuck on the cell, since the cell could not move, and the MC was fixed to the cell. Another MC could be moved by the

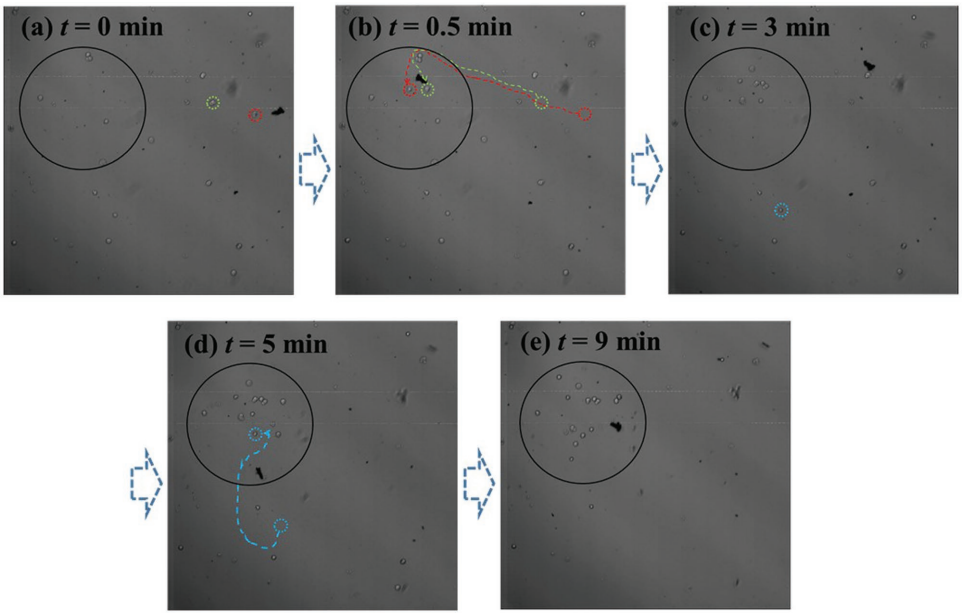

Figure 10. Snapshots of collecting PC3 cells to a target area (denoted by the black circle) by an MC actuated using a nonuniform AC B-field.

nuAMF to the vicinity of this cell, and would join the previous MC to form a larger MC as shown by $t = 25$ s in Figure 11b. The moving trajectory of the MC is marked as the red dash line in the figure of $t = 0$ s. Such a larger MC formation is due to the magnetic attraction between the two MCs. With more and more MCs were directed to the cell, the size of MC kept increasing, as shown in snapshots in Figure 11. Such a process could be used to exert a larger magnetic force/torque at a specific point of the cell and to eventually move the attached cell or rapture the cell membrane. Recently, Mazuel et al. performed a similar experiment by assembling polymer–iron oxide hybrid nanorods on cell membrane and demonstrated the free rotation of these rods as a biomagnetic torsion pendulum.[29] In addition, the accumulation of MNRs on a cell is relevant to targeted drug delivery. For example, by loading anticancer drugs onto these Fe_3O_4 nanorods (NRs), using the magnetic manipulation system, the loaded NRs can be directed to and directly interact with the target cell without affecting other cells.

3. Conclusions

In this work, we demonstrate that, with a programmable keyboard system to control four spatially arranged solenoids, the

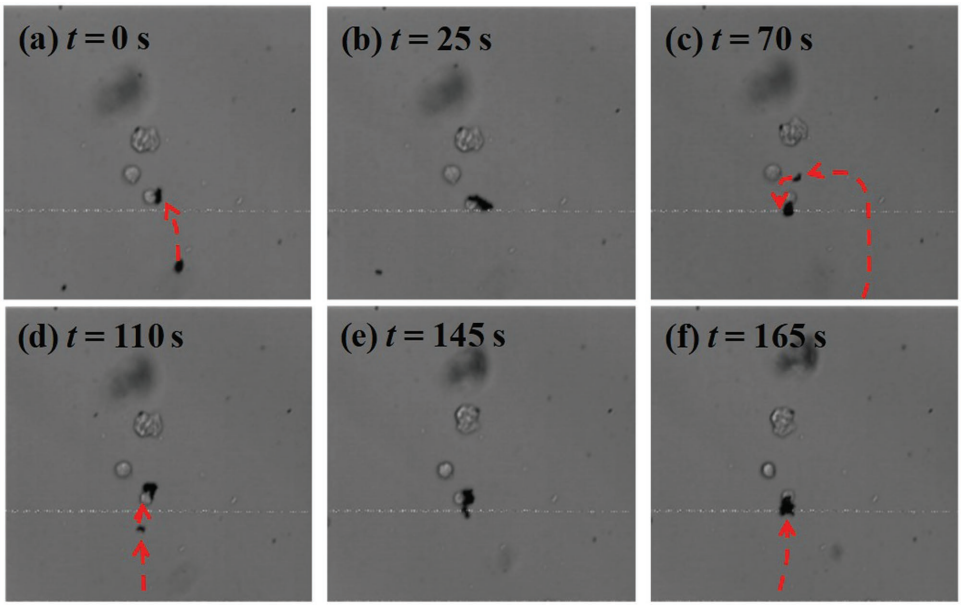

Figure 11. Snapshots of accumulating MCs onto an A549 cell.

motion of an MNR/MC under a nuAMF is highly directional and controllable. MCs actuated by a nuAMF can be used for single cell manipulation. The manipulation process can be divided into five stages, approaching, pushing, carrying, dragging, and releasing. The effect of the B-field frequency on cell manipulation was investigated systematically. Other applications of cell manipulation, such as concentrating cells at a target position and bringing MCs onto a single cell, have also been demonstrated.

The cell manipulation method demonstrated here is a noncontact method because the MC and cell do not get into contact and the hydrodynamic interaction between them is responsible for the observed cell movement. Compared to the existing magnetic single cell manipulation methods, it offers several advantages. First, compared to particle manipulation by magnetophoresis, actuation by nuAMF requires much less power to achieve the same translational speed and offers more flexibility in operation because, besides B-field gradients, parameters such as the frequency of the B-field and the shape of MNR/MC can also be used to tune the speed of an MNR/MC. Second, it realizes precise manipulation of nonmagnetic particles and cells along arbitrary, reconfigurable paths in 2D space at a low cost (the cost of the setup in this work is less than $500 if microscope and computer are not included), which is difficult to achieve using other methods. The cell manipulation method reported here thus helps advance the state-of-the-art of single-particle manipulation in liquid environment. Third, in addition to magnetic field and field gradient, other parameters such as size and shape of MC, and the field frequency can be used to control the motion of the MC. Finally based our experimental data and mechanistic understanding from numerical model, the MC–cell interaction is noncontact, which is a plus for biological applications.

Clearly here we focus on the proof of principle demonstration of cell manipulation and MC trapping, and try to gain some fundamental understanding of the MC–cell interaction during the manipulation process. We have not yet touched more advanced manipulations such as patterned cell manipulation, multiple/parallel cell manipulations, cell recognition, etc., which may require advanced microfluidic fabrication and better magnet design/control. Also, the biological activities of the manipulated cells such as biocompatibility, cell death, tissue formation, etc., are important and have not been addressed. We will address these issues with followed works in the future.

4. Experimental Section

Fabrication and Characterization of Ni MNRs and Fe_3O_4 MNRs: Ni MNRs were fabricated by the oblique angle deposition method.[30] A monolayer of 2 μm diameter polystyrene (PS) bead was first prepared on Si substrates using an air-liquid interface method.[31] The monolayer covered Si substrates were then loaded into a custom-built electron beam evaporation chamber. Nickel (Alfa Aesar) was deposited at a vapor incident angle of 86° and at a rate of ≈0.5 nm s^{-1}, monitored by a quartz crystal microbalance (QCM) facing directly toward the incident vapor. Ni MNRs of length ≈1 μm were obtained when the QCM reading reached 2 μm. Figure 1a shows a representative SEM image of a single Ni MNR dispersed in water.

The Fe_3O_4 MNRs were synthesized by a hydrothermal method following by an annealing/reducing process.[25] Briefly, 75 mL 0.02 M $FeCl_3{\cdot}6H_2O$ (Acros Organics) and 0.45×10^{-3} M NaH_2PO_4 (Sigma) aqueous solutions were thoroughly mixed and then transferred into a 100 mL autoclave. After being maintained at 160 °C in an oven for 12 h and cooled down to room temperature, the resulting Fe_2O_3 NRs were collected and washed by centrifugation. The overnight dried Fe_2O_3 NRs were annealed in N_2 carried ethanol flow at 350 °C for 1 h to obtain the Fe_3O_4 MNRs. The crystal structure, morphology, composition as well as the magnetic property of the resulting Fe_2O_3 and Fe_3O_4 NRs were characterized by different techniques, and details were reported in ref. [25]. When the Fe_3O_4 MNRs were dispersed in water, they formed MCs due to their ferromagnetic property. In Figure 1b, a representative MC with length of ≈11 μm and width of ≈3 μm is shown, consisted of many uniform sized ellipsoid Fe_3O_4 MNRs. These ellipsoid MNRs have an average length of 300 ± 40 nm and an average diameter of 50 ± 7 nm, as revealed by the transmission electron microscope (TEM) image shown in the inset image of Figure 1b.

Cell Cultures: PC3 cells were maintained in Ham's F12 medium (SH30526, GE Healthcare Life Sciences, Logan, Utah) and minimum essential medium (MEM, M8042, Sigma-Aldrich, St Louis, MO), respectively, with 5% fetal bovine serum (FBS, F2442, Sigma-Aldrich, St Louis, MO) and 100 U mL^{-1} penicillin–streptomycin (SV30010, GE Healthcare Life Sciences, Logan, UT) in a 37 °C, 5% CO_2 humidified environment. The cultured cells were maintained at a subconfluence condition with passaging every 2–3 days.

A549 lung cancer cells (ATCC, Manassas, VA) were cultured in RPMI-1640 medium (Mediatech, Inc., Manassas, VA) supplemented with 10% (v/v) FBS (Life Technologies, Carlsbad, CA) and 1% (v/v) penicillin/streptomycin solution (Mediatech, Inc., Manassas, VA) at 37 °C under a humidified atmosphere of 5% CO_2. Cells were released through incubation with 0.05% Trypsin–EDTA solution (Life Technologies, Carlsbad, CA) at 37 °C for 5–10 min.

Magnetic Manipulation System: As shown in Figure S2 of the Supporting Information, the B-fields for the MNR/MC motion and cell manipulation were generated by four solenoids (Air-core Solenoid #14825, Science Source, Waldoboro, ME) with cast iron cores.[25] These solenoids were connected to two 2-channel current supplies (PLX3602, QSC) with input signals with a specific frequency f_H from 5 to 20 Hz and the amplitude of the current I_0 = 2 A from a function generator (33220A, Agilent). Four solenoids were programmed with on–off AC currents via a four-channel sound card in a computer to control MCs' motion in four horizontal directions. A MATLAB program was created to use four keyboard strokes (e.g., "a" "s" "w" "z") to drive an MC to move left, right, forward, and backward and to control the frequency and amplitude of the AC current in each solenoid (see Movie S1, Supporting Information). The travel distance of an MC depends on how long the corresponding key is pressed.

To determine the MNR/MC moving resolution, Ni MNRs with a mass concentration of 0.01 mg mL^{-1} was used. The concentration of the Fe_3O_4 MNRs used in all cell manipulation experiments is 0.01 mg mL^{-1}. A droplet of 20 μL cell suspension from their original growth medium with a concentration of $\approx 1 \times 10^3$ cell mL^{-1} was first dispersed onto a precleaned Si substrate (1 in × 1 in) which was placed in the center of the four-solenoids system (approximately about 5 cm away from the front surface of each solenoid's iron core). Then a droplet of 20 μL Fe_3O_4 MNRs suspension in the same growth medium was added to the cell droplet. All movies were obtained by a fast CCD camera (Phantom v9.1) with a frame rate of 20 fps through the microscope with a 10× objective lens. During the experiment, no significant temperature changes of the samples were noticed. An in-house cluster tracking MATLAB program was used to analyze the movies (see Section S3, Supporting Information).[25]

Statistic Analysis: To analyze the size of Fe_3O_4 MNRs, measurements on more than 100 MNRs randomly selected from different SEM images were performed, and then the average was taken, and the standard deviation for the length and diameter was computed. For MNR/MC motion speed and directionality characterizations as well as cell manipulation speed, more than ten stable trajectories (no lost tracks happened, and tracking time greater than 10 s) from different

MCs/cell manipulations were tracked and analyzed, and the corresponding average values and standard deviation were obtained.

Supporting Information

Supporting Information is available from the Wiley Online Library or from the author.

Acknowledgements

L.Z., W.H., and Y.Z. were funded by the National Science Foundation under Contract Nos. ECCS-1609815 and ECCS-1808271. L.M. and W.Z. acknowledge funding from the National Institutes of Health (NIH R21GM104528 and UL1TR002378), and the National Science Foundation (Award No. 1150042). R.Q. acknowledges support by the NSF under grant number 1808307.

Conflict of Interest

The authors declare no conflict of interest.

Keywords

alternating magnetic field, Fe_3O_4, magnetic clusters, magnetic nanorods, single cell manipulation

Received: August 28, 2018
Revised: September 26, 2018
Published online: October 17, 2018

[1] A. Ashkin, J. Dziedzic, *Science* **1987**, *235*, 1517.
[2] H. Zhang, K.-K. Liu, *J. R. Soc., Interface* **2008**, *5*, 671.
[3] O. Guillaume-Gentil, E. Potthoff, D. Ossola, C. M. Franz, T. Zambelli, J. A. Vorholt, *Trends Biotechnol.* **2014**, *32*, 381.
[4] C. R. Cabrera, P. Yager, *Electrophoresis* **2001**, *22*, 355.
[5] G. Vieira, T. Henighan, A. Chen, A. Hauser, F. Yang, J. Chalmers, R. Sooryakumar, *Phys. Rev. Lett.* **2009**, *103*, 128101.
[6] M. S. Sakar, E. B. Steager, D. H. Kim, M. J. Kim, G. J. Pappas, V. Kumar, *Appl. Phys. Lett.* **2010**, *96*, 043705.
[7] M. Zborowski, J. J. Chalmers, W. G. Lowrie, in *Microtechnology for Cell Manipulation and Sorting* (Eds: W. Lee, P. Tseng, D. Di Carlo), Springer International Publishing, Cham, Switzerland **2017**, pp. 15–55.
[8] T. Henighan, A. Chen, G. Vieira, A. J. Hauser, F. Y. Yang, J. J. Chalmers, R. Sooryakumar, *Biophys. J.* **2010**, *98*, 412.
[9] D.-H. Kim, E. A. Rozhkova, I. V. Ulasov, S. D. Bader, T. Rajh, M. S. Lesniak, V. Novosad, *Nat. Mater.* **2010**, *9*, 165.
[10] E. B. Steager, M. S. Sakar, C. Magee, M. Kennedy, A. Cowley, V. Kumar, *Int. J. Rob. Res.* **2013**, *32*, 346.
[11] V. H. Ho, K. H. Müller, A. Barcza, R. Chen, N. K. Slater, *Biomaterials* **2010**, *31*, 3095.
[12] K. Ino, A. Ito, H. Honda, *Biotechnol. Bioeng.* **2007**, *97*, 1309.
[13] B. M. Mattix, T. R. Olsen, M. Casco, L. Reese, J. T. Poole, J. Zhang, R. P. Visconti, A. Simionescu, D. T. Simionescu, F. Alexis, *Biomaterials* **2014**, *35*, 949.
[14] S. Ghosh, S. R. P. Kumar, I. K. Puri, S. Elankumaran, *Cell Proliferation* **2016**, *49*, 134.
[15] V. Du, N. Luciani, S. Richard, G. Mary, C. Gay, F. Mazuel, M. Reffay, P. Menasché, O. Agbulut, C. Wilhelm, *Nat. Commun.* **2017**, *8*, 400.
[16] J. R. Basore, L. A. Baker, *Anal. Bioanal. Chem.* **2012**, *403*, 2077.
[17] P. Rinklin, H.-J. Krause, B. Wolfrum, *Lab Chip* **2016**, *16*, 4749.
[18] D. Robert, N. Pamme, H. Conjeaud, F. Gazeau, A. Iles, C. Wilhelm, *Lab Chip* **2011**, *11*, 1902.
[19] H. Lee, A. M. Purdon, R. M. Westervelt, *Appl. Phys. Lett.* **2004**, *85*, 1063.
[20] S. Martel, C. C. Tremblay, S. Ngakeng, G. Langlois, *Appl. Phys. Lett.* **2006**, *89*, 233904.
[21] H. Rostaing, H. Chetouani, M. Gheorghe, P. Galvin, *Sens. Actuators, A* **2007**, *135*, 776.
[22] Q. Cao, X. Han, L. Li, *Lab Chip* **2014**, *14*, 2762.
[23] F. Gertz, A. Khitun, *Phys. Proc.* **2016**, *82* (Supplement C), 8.
[24] F.-G. Tseng, T. S. Santra, *Essentials of Single-Cell Analysis: Concepts, Applications and Future Prospects, Series in BioEngineering*, Springer, Berlin **2016**.
[25] W. Huang, F. Yang, L. Zhu, R. Qiao, Y. Zhao, *Soft Matter* **2017**, *13*, 3750.
[26] R. Kerssebaum, *DOSY and Diffusion by NMR*, Bruker BioSpin GmbH, Rheinstetten, Germany **2006**.
[27] COMSOL, COMSOL Multiphysics User's Guide, Version: 5.1 **2015**.
[28] C. Wang, J. Chen, T. Talavage, J. Irudayaraj, *Angew. Chem., Int. Ed.* **2009**, *48*, 2759.
[29] F. Mazuel, S. Mathieu, R. Di Corato, J.-C. Bacri, T. Meylheuc, T. Pellegrino, M. Reffay, C. Wilhelm, *Small* **2017**, *13*, 1701274.
[30] Y. He, J. Fu, Y. Zhang, Y. Zhao, L. Zhang, A. Xia, J. Cai, *Small* **2007**, *3*, 153.
[31] G. K. Larsen, Y. He, W. Ingram, Y. Zhao, *Nano Lett.* **2013**, *13*, 6228.

